ELSEVIER

Journal of Nuclear Materials 299 (2001) 140–147

journal of nuclear materials

www.elsevier.com/locate/jnucmat

Computer simulation of Pu^{3+} and Pu^{4+} substitutions in gadolinium zirconate

R.E. Williford *, W.J. Weber

Materials Department, Pacific Northwest National Laboratory, M.S. K2-44, P.O. Box 999, Richland, WA 99352, USA

Received 20 November 2000; accepted 9 August 2001

Abstract

Atomistic computer simulations have been used to determine the energetics of a variety of defect reactions related to the incorporation of Pu^{3+} and Pu^{4+} into the pyrochlore and the fluorite-type structures of $Gd_2Zr_2O_7$. The lowest energy states were found for Pu^{3+} substitutions on Gd sites in the pyrochlore (−1.00 eV/Pu) and the fluorite-type (−1.55 eV/Pu) structures, so these defect reactions are the most likely configurations under reducing conditions that favor Pu^{3+} ions. Slightly higher, but still exothermic, energies (−0.26 to −0.45 eV) were calculated for Pu^{4+} substitutions on Zr sites for several fluorite-type cases, indicating that oxidizing conditions should favor Pu^{4+} incorporation on Zr sites in $Gd_2Zr_2O_7$ hosts. Defect reactions involving cation vacancies or interstitials exhibited significantly higher energies, and are therefore not expected to occur. Mean field calculations indicated that the increases in crystal volume associated with Pu incorporation are minimized by the excess free volume associated with the Gd site in the pyrochlore structure. Volume changes upon thermal phase transformation from fluorite to pyrochlore are smaller for the material incorporating Pu by substitution than for the virgin material, with a slight advantage for the reducing conditions associated with Pu^{3+} substitutions on Gd sites.

PACS: 61.80.−X; 61.80.AZ; 61.82.MS

1. Introduction

Immobilization of fissile Pu generated by the nuclear fuel cycle or recovered from nuclear weapons is an important environmental challenge [1,2]. Within a few years, the amount of separated Pu generated by the reprocessing of commercial reactor fuel will exceed military inventories [3]. Current strategies around the world include immobilizing the Pu in a stable host matrix and either 'burning' it in a nuclear reactor or placing it in a geologic repository for permanent storage. For geologic storage, the primary host matrix currently being considered is gadolinium titanate ($Gd_2Ti_2O_7$) with the pyrochlore ($A_2B_2O_7$) structure [4]. Under α-decay irradiation, Gd-titanate transforms to an amorphous structure that enhances the measured aqueous dissolution rate of Pu by a factor of 50 [5,6]. Recently [7], the pyrochlore system based on gadolinium zirconate ($Gd_2Zr_2O_7$) has been found to be systematically more resistant than Gd-titanate to irradiation-induced amorphization. This behavior has since been confirmed in erbium zirconate ($Er_2Zr_2O_7$) with the related fluorite-type structure [8]. Heavy-ion irradiation of Gd-zirconate causes an order–disorder transformation to a radiation-resistant fluorite structure. The Gd-zirconate's fluorite structure is identical to that of stabilized cubic zirconia, which is known to exhibit high resistance to radiation effects.

The purpose of this paper is to quantify the energetics of Pu^{3+} and Pu^{4+} incorporation (by substitutions and interstitials) into the $Gd_2Zr_2O_7$ pyrochlore and fluorite-type structures, so that waste host processing and stability issues may be better understood, in a manner similar to prior work on zircon [9]. Future work using similar computational methods will address phase transformations and the migration energetics of

* Corresponding author. Tel.: +1-509 375 2956; fax: +1-509 375 2186.

E-mail address: re_williford@pnl.gov (R.E. Williford).

0022-3115/01/$ - see front matter
PII: S0022-3115(01)00687-0

vacancies, interstitials, and impurities in relation to radiation damage and leach resistance.

2. Computational methods and interatomic potentials

The general utility lattice program (GULP) [10,11] was used to simulate the energetics and structures of perfect and defective lattices. Because this and several similar computer codes have been thoroughly described many times in the literature, the following description will be brief. GULP uses an energy minimization method based on the Born model, and is unique in its use of crystal symmetry to speed up calculations. Isolated defects in extended solids were addressed with the Mott–Littleton approximation [12], with a Region 1 radius of 0.9 nm. Ionic polarization was treated using the Dick–Overhauser shell model [13], including the important repulsion–polarization coupling that prevents excessive polarization. Elemental defect energies were calculated by standard methods [14], and subsequently used to calculate the energetics of more complex defect reactions that included charge neutrality. All energy minimization calculations were performed at 0 K.

At higher temperatures, simulations were performed with the DL_POLY molecular dynamics code [15]. DL_POLY is actually a package of routines designed for the simulation of a wide variety of molecular systems. It contains a number of potential forms, boundary conditions, and integration algorithms that can be applied at the user's discretion. In the present study, supercell models with 704 atom cores were used in simulations to determine lattice energies as a function of temperature. All simulations were performed using a Berendson NPT (constant pressure) ensemble with periodic boundary conditions. The temperature was raised in steps of 500 K, and equilibration periods of at least 10 000 time steps at 0.5 fs per step were performed at each intermediate temperature. As in the energy minimization calculations, Coulombic forces were calculated with the standard Ewald sum technique.

The interatomic potentials employed for Gd–O and O–O were previously used for the pyrochlore phase [16–19], thus providing a foundation for the present work. A new rigid-ion Zr–O potential was developed for the present work by simultaneously fitting the potential parameters to structural data for the ZrO_2 cubic (Fm3m) and tetragonal (P42/nmc) phases [20], with averaged oxygen core and shell charges from previous work on $Gd_2Zr_2O_7$ [18], where two distinct 'species' of oxygen charges had been used to represent the 48f and 8a oxygen sites in the pyrochlore. Potentials for Pu^{3+}–O and Pu^{4+}–O were previously developed [9] by fitting to the structures and available properties of Pu_2O_3 and PuO_2. In the present work, the Pu^{3+}–O potential was further refined by fitting the Buckingham A parameter to the measured lattice constant of $Pu_2Zr_2O_7$ [21]. In all cases, the radial cutoff distance for the potentials was 1.0 nm. The interatomic potential parameters are given in Table 1.

Table 1
Parameters for interatomic potentials used in this work

	Potential		
	A (eV)	ρ (nm)	C (10^{-6} eV nm^6)
Gd–O	1336.7600	0.03551	0.0
Zr–O	1019.4250	0.03746	0.0
O–O	22764.0000	0.01490	27.89
Pu^{3+}–O	3529.7612	0.03148	0.0
Pu^{4+}–O	806.4236	0.04141	0.0

Formal charges were used for all ions to facilitate charge balancing for defect calculations. All potentials were rigid ion models except oxygen and gadolinium, which had shell charges of −2.3194 and −0.25 |e|, and core-shell spring constants of 26468.7 and 14500.0 eV/nm^2, respectively. The oxygen and gadolinium shell models were needed to reproduce the available physical properties of $Gd_2Zr_2O_7$. The rigid ion form was used for zirconium and plutonium species for two reasons. The first was to facilitate other calculations using the molecular dynamics method. The second reason was that there seemed to be no advantage to including the shells for zirconium: no marked improvement in predicted crystal properties could be realized when available data bases were used to fit the shell models. The Buckingham form was used for all potentials

$$E = A\exp(-r/\rho) - C/r^6. \tag{1}$$

This familiar potential is employed quite often in energy minimization work, so its use here facilitates comparison to the literature. Other potential forms are also possible, but would not be expected to change the results appreciably because they all must be fit to the same data base of material properties. The calculated lattice parameters based on these interatomic potentials are in good agreement with experimental values, as shown in Table 2.

3. Formation energies for phases and elemental defects

Mean field energy minimization calculations were used to determine the equilibrium lattice energies at 0 K for the ideal pyrochlore (−32.13 eV/atom) and fluorite (−27.37 eV/atom) phases of $Gd_2Zr_2O_7$. The 4.76 eV/atom energy difference between the two phases at absolute zero is consistent with phase diagrams [22], but is substantially larger than that estimated from calorimetry experiments (0.10 eV/atom at 975 K) [22]. Molecular dynamics using DL_POLY [15] and the

Table 2
Comparison between experimental and calculated lattice constants for $Gd_2Zr_2O_7$, Gd_2O_3, ZrO_2, Pu_2O_3, PuO_2 and $Pu_2Zr_2O_7$

Material/parameter	Experiment	Calculation
$Gd_2Zr_2O_7$ (Fm3m)		
a, b, c (nm)	0.5263	0.5260
$Gd_2Zr_2O_7$ (Fd3m)		
a, b, c (nm)	1.0520	1.0521
$Pu_2Zr_2O_7$ (Fd3m)		
a, b, c (nm)	1.0692	1.0689
Gd_2O_3 (I213)		
a, b, c (nm)	1.0790	1.0719
ZrO_2 (Fm3m)		
a, b, c (nm)	0.5090	0.5096
ZrO_2 (P42/nmc)		
a, b (nm)	0.3601	0.3603
c (nm)	0.5179	0.5173
Pu_2O_3 (P-3m1)		
a, b (nm)	0.3838	0.3918
c (nm)	0.5918	0.6005
PuO_2 (Fm3m)		
a, b, c (nm)	0.5397	0.5459

Table 3
$Gd_2Zr_2O_7$ defects and lattice formation energies, eV

Defect	Fluorite cluster	Fluorite unit cell	Pyrochlore
Pu_{Gd}^{3+}	0.07	0.94	0.62
Pu_{Zr}^{4+}	7.66	7.47	8.59
$Pu_{Zr'}^{3+}$	36.45	36.51	38.82
$Pu_{Gd\cdot}^{4+}$	−27.53	−27.36	−26.77
$V_O^{\cdot\cdot}$	14.97	24.45	18.38 (48f)
$V_{Zr}^{''''}$	85.05	84.68	86.39
$V_{Gd}^{''''}$	48.16	48.38	46.49
O_{V_O}''	−15.53	−14.96	−13.90
$Zr_i^{''''}$	−67.71	−69.66	−57.03
$Pu_i^{4+\,'''}$	−58.42	−59.19	−55.17
$Pu_i^{3+\,'''}$	−32.44	−30.82	−28.70
Lattice			
ZrO_2^L (Fm3m)	−109.49		
$Gd_2O_3^L$	−132.79		
PuO_2^L	−101.57		
$Pu_2O_3^L$	−129.55		

potentials in Table 1 were used to determine lattice energies for both phases as functions of temperature up to the temperature of the calorimetry experiments. The results indicate that the total energy difference is 0.15 eV/atom at 975 K, in good agreement with experiment [23]. A similar result would be expected using *free* energy minimization at higher temperatures. This small energy difference is consistent with the long annealing process that is required below the phase transition temperature (1803 K) to form the completely ordered pyrochlore structure [7,24].

The calculated formation energies of elemental defects are shown in Table 3 using Kroeger–Vink notation. The formation energies of the relevant crystal lattices (Table 3) are denoted by the superscript L. Defect calculations for the pyrochlore structure were straightforward, but the partial occupancies in the fluorite structure (e.g., 0.875 for oxygen) required that atom-explicit formula units be defined for proper charge balance in the defect calculations. The atom-explicit formula unit for each fluorite model was embedded in a mean-field infinite crystal using the Mott–Littleton method [12]. Two such fluorite cases were treated for comparison, as follows. The first case assumed that the four explicit cations occurred in a small cluster centered around a vacant oxygen site, forming a cation tetrahedron as shown in Fig. 1. Seven more of the closest oxygen sites were defined explicitly with occupancies of unity instead of the 0.875 value used in the mean field calculations. The second fluorite case assumed that the four explicit cations were placed on a (1 0 0) plane around the periphery of a unit cell, with the two explicit Gd opposite each other, and likewise for the two explicit

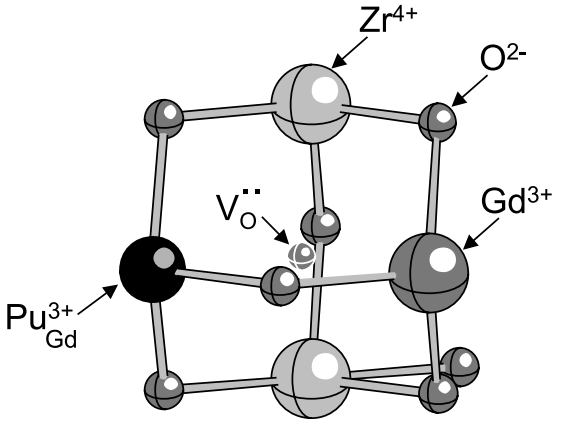

Fig. 1. Atom-explicit formula unit for Pu^{3+} on Gd site in the fluorite cluster model.

Zr. Seven of the oxygen sites in the unit cell were defined with an occupancy of unity, while the eighth was defined as a vacancy for charge balance. Consequently, the second fluorite case, which is shown in Fig. 2, consisted of a slightly larger atom–explicit cluster (0.53 nm diameter) than the first case (0.39 nm diameter). The same potentials were used in all cases.

The defect formation energies given in Table 3 are generally consistent between the three cases, by virtue of similar magnitudes. However, the oxygen vacancy formation energy for the fluorite unit-cell model is higher than for the cluster model because the cluster model had four explicit cations around the O vacancy site, whereas the unit-cell model had only two explicit and two mean

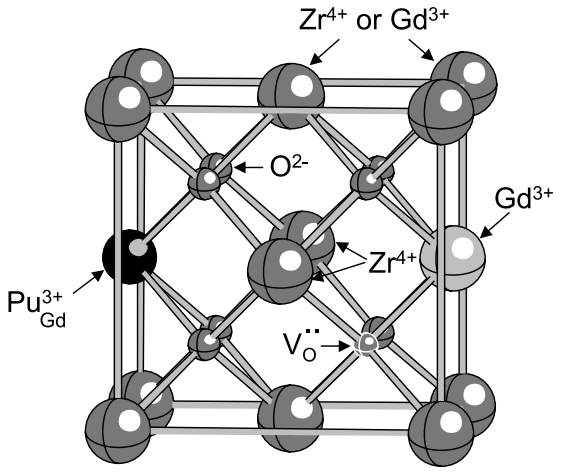

Fig. 2. Atom-explicit formula unit used for Pu^{3+} on a Gd site in the fluorite unit-cell model.

field cations around the O vacancy. This is due to the larger size of the explicit-atom region in the unit-cell model; consequently, a comparable defect geometry could not be obtained with four explicit cations on the (1 0 0) plane. The oxygen vacancy for the pyrochlore was chosen to occur at a 48f site (Fig. 3), rather than an 8a site, because of its lower formation energy in the ordered material [18]. The additional oxygen anions required for charge balancing in the next section were allowed to fill vacant oxygen sites by substitution, rather than being added as interstitials at a higher energy expense, and are denoted O''_{V_O}. The sites selected for the additional oxygen occupancy were the normally vacant 8b site in the pyrochlore and the explicit oxygen vacancies in the fluorite cases described above.

4. Energies of Pu^{3+} and Pu^{4+} substitutions and interstitials with charge compensation

The most likely configuration of defects can be determined by defining defect reaction equations and computing the resultant energies, using the perfect oxide lattices in Table 3 as reference states. This is a common approach for static energy minimization calculations, and often supplies a variety of possible defect reactions for consideration. Twelve possible defect reactions were considered: four for Pu^{3+}_{Gd} substitutions and Pu^{3+}_{i} interstitials, four for Pu^{4+}_{Zr} substitutions and Pu^{4+}_{i} interstitials, and four involving Pu^{3+}_{Zr} and Pu^{4+}_{Gd} substitutions. Defect reaction equations for each case are given in Appendix A.

Table 4 lists the energies of these defect reactions in order of decreasing preference (increasing energy) for the fluorite cluster model, in terms of eV per Pu ion incorporated into the lattice. The negative (exothermic) energy for Pu^{3+} substitution on a Gd site (Reaction 1) may indicate that reducing atmospheres, which favor Pu^{3+}, may enhance Pu incorporation into $Gd_2Zr_2O_7$ hosts. Analogously, under oxidizing conditions, the more oxidized Pu^{4+} state prefers, energetically, to be incorporated on Zr sites in either phase by simple substitution (Reaction 3).

Pu^{3+} can occupy a Zr^{4+} site, with charge compensation by oxygen vacancies, with an energy of −0.78 eV for the fluorite cluster model (Reaction 2). While Reaction 2 is not as energetically favored as substitution of Pu^{3+} on Gd sites, it is nevertheless exothermic. Consequently, Pu^{3+} may occur on both Gd and Zr sites in the fluorite cluster model. This is not true for the fluorite unit-cell model or for the pyrochlore model because Reaction 2 in Table 4 is endothermic for those cases, with higher

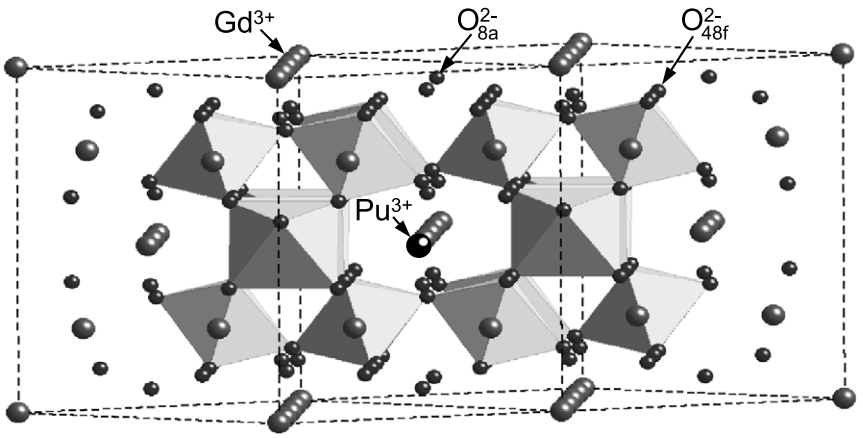

Fig. 3. Pu^{3+} on a Gd site in the pyrochlore model. Polyhedral representation of the pyrochlore structure, showing ZrO_6 octahedra in a $2 \times 1 \times 1$ supercell along the $\langle 1\,1\,0 \rangle$ axis. Zr atoms are not shown for clarity. The small spheres at each octahedron corner are the 48f oxygen atoms. The larger isolated spheres are Gd atoms. The small isolated spheres above and below the A rows are oxygen atoms in the 8a positions.

Table 4
Defect reaction energies, eV/Pu

Reaction	Description	Fluorite cluster	Fluorite unit cell	Pyrochlore
1	Pu_{Gd}^{3+}	−1.55	−0.68	−1.00
2	$Pu_{Zr}^{3+\prime} + 0.5V_{O}^{\cdot\cdot}$	−0.78	4.02	1.59
3	Pu_{Zr}^{4+}	−0.26	−0.45	0.67
4	$Pu_{Gd}^{4+\cdot} + 0.5O_{V_O}^{\prime\prime}$	−0.12	0.34	1.45
5	$Pu_{Gd}^{4+\cdot} + 0.33V_{Gd}^{\prime\prime\prime\prime}$	1.57	1.81	1.77
6	$Pu_{Zr}^{3+\cdot} + 0.25Zr_{i}^{\prime\prime\prime\prime}$	2.18	1.75	7.22
7	$Pu_{Gd}^{3+} + Pu_{i}^{3+\cdots} + V_{Gd}^{\prime\prime\prime}$	6.27	5.13	7.58
8	$Pu_{i}^{3+\cdots} + 1.5O_{V_O}^{\prime\prime}$	9.04	11.52	15.23
9	$Pu_{i}^{4+\cdots\cdot} + V_{Zr}^{\prime\prime\prime\prime} + Pu_{Zr}^{4+}$	9.23	8.56	11.98
10	$Pu_{i}^{4+\cdots\cdot} + 2O_{V_O}^{\prime\prime}$	12.13	12.46	18.60
11	$Pu_{i}^{3+\cdots} + V_{Gd}^{\prime\prime\prime}$	14.10	10.94	16.17
12	$Pu_{i}^{4+\cdots} + V_{Zr}^{\prime\prime\prime\prime}$	18.71	17.57	23.32

energy cost. Some reduction in the reaction energy could be expected if the Pu^{3+} is incorporated as a cluster consisting of two Pu^{3+} ions on near-neighbor Zr^{4+} sites with a nearby charge-compensating oxygen vacancy, as reported for the case of zircon [9]. However, such detailed calculations were not possible in this paper because the size requirements for the fluorite models exceeded the memory allocations of the GULP code.

Substitution of Pu^{4+} on Gd^{3+} sites, with charge compensation by oxygen filling a normally vacant oxygen site (Reaction 4), is also possible for the fluorite cluster because of the exothermic reaction energy (−0.12 eV) in Table 4. The fluorite unit-cell model shows a slightly endothermic energy (0.34 eV) for this case, while the pyrochlore structure case exhibits a larger endothermic energy of 1.45 eV. Incorporation of Pu^{4+} on Gd^{3+} sites as a defect cluster, consisting of two Pu^{4+} ions on near-neighbor Gd^{3+} sites with a charge compensating oxygen filling a nearby vacant oxygen site, would also be expected to reduce the reaction energy, but such calculations were again not possible. The remaining reactions (5–12) in Table 4 are not likely to occur because they involve cation vacancies or interstitials, which exhibit much higher formation energies. In an experimental situation, the most likely defect reaction to be measured is the one with the lowest energy. However, some of the scatter in experimental data could be caused by other reactions with similar energetics, especially for exothermic reactions.

5. Unit-cell volume and lattice energy changes

Several mean field calculations were performed (using partial occupancies of atomic sites in GULP) to investigate the volume and lattice energy changes associated with the defect reactions of lowest energy: 10% Pu^{3+} and 10% Pu^{4+} substitutions on Gd and Zr sites, respectively. The computed volumes per atom and lattice-averaged energies per atom at 0 K are shown in Table 5. The propensity for the formation of the pyrochlore phase at lower temperatures is indicated by the lower energy per atom.

Crystal volume and lattice energy increases at 0 K (relative to the pristine lattices) caused by incorporating Pu by substitution are shown in Table 6. Note that although these processes would not actually occur at absolute zero, energy minimization is often used to predict the trends to be expected. The smallest energy changes occur for Pu^{3+} substitutions on Gd sites, indicating that reducing conditions associated with the Pu^{3+} ion could facilitate Pu incorporation. This is consistent with the defect reactions in Table 4. However, note that the fluorite (Fm3m) structure exhibited the lowest *defect* energies for Pu^{3+} on Gd and Pu^{4+} on Zr substitutions in Table 4, whereas the pyrochlore (Fd3m) structure is energetically preferred in the *mean field* calculations of Table 6. Both the defect and the mean field calculations were performed at constant pressure. However, the de-

Table 5
Computed atomic volumes and lattice energies per atom at 0 K for 10% Pu_{Gd}^{3+} and 10% Pu_{Zr}^{4+} substitutions in the pyrochlore (Fd3m) and fluorite (Fm3m) phases of $Gd_2Zr_2O_7$

Structure	Substitution	Volume/atom (nm^3)	Energy/atom (eV)
Fm3m	None	0.01213	−27.368
Fd3m	None	0.01323	−32.129
Fm3m	Pu_{Gd}^{3+}	0.01238	−27.291
Fd3m	Pu_{Gd}^{3+}	0.01331	−32.115
Fm3m	Pu_{Zr}^{4+}	0.01239	−27.138
Fd3m	Pu_{Zr}^{4+}	0.01338	−31.964

Table 6
Volume and lattice energy increases at 0 K caused by 10% Pu incorporation, referenced to the pristine lattices with no substitutions

Structure	Substitution	Radius ratio (Pu/native)	Volume/atom increase (%)	Energy/atom increase (%)
Fm3m	Pu^{3+}_{Gd}	1.06	2.06	0.28
Fd3m	Pu^{3+}_{Gd}	1.06	0.61	0.05
Fm3m	Pu^{4+}_{Zr}	1.14	2.14	0.85
Fd3m	Pu^{4+}_{Zr}	1.19	1.13	0.52

fect calculations treated a small number of localized defects embedded in a perfect infinite crystal, which provided some measure of volumetric constraint for the localized defect region. Conversely, in the mean field calculations in Table 6, the entire infinite medium expanded to relieve the internal strains associated with the infinite number of Pu substitutions in the infinite crystal. Even disregarding the differences in the number density of substitutions, it must be recognized that these are two distinctly different types of calculations. The energies in Table 4 are individual defect formation energies, while those in Table 6 are lattice energies per atom (averaged over all atoms in the lattice). Care must be taken when comparing the two because the above results can be misinterpreted as giving conflicting conclusions, which is not the case. Under experimental conditions, a sufficient number of defects would be required for volume changes to be measurable, so the mean field results are most applicable to actual conditions.

Increases in volume and lattice energy per atom in Table 6 are larger for the fluorite structure than for the pyrochlore structure, for reasons that become clear when the ionic radii are compared, as follows. Pu^{4+} is sixfold coordinated in the pyrochlore and eightfold coordinated in the fluorite, with radii of 0.0860 and 0.0960 nm, respectively. Pu^{3+} is eightfold coordinated in both phases, but only the sixfold coordinated case is documented [25], with a radius of 0.1000 nm. The eightfold coordinated radius of Pu^{3+} was estimated from the Pu^{4+} data as $0.1000 \times 0.0960/0.0860 = 0.1116$ nm. This agrees with the value of 0.112 nm given for $Pu_2Zr_2O_7$ [21]. The radius of the Gd^{3+} ion in the fluorite and in the pyrochlore is 0.1053 nm. The Zr^{4+} ionic radius in the fluorite is 0.084 and 0.072 nm in the pyrochlore. The increasing ionic radius ratios (Pu/native ion) in Table 6 are generally consistent with increases in the lattice-averaged energy per atom, i.e., Pu^{4+}_{Zr} substitutions cause greater energy increases than Pu^{3+}_{Gd} substitutions. The radius ratios are consistent with the increases in volume per atom for the pyrochlore, but are less well defined for the fluorite. The reason is that the Gd and Zr share partial occupation of the same crystallographic site (the 'A' site) in the fluorite, but occupy different sites in the pyrochlore (Gd occupies 'A' sites in $A_2B_2O_7$, Zr occupies 'B' sites). Consequently, the difference between the two substitutions is attenuated by their random locations in the fluorite lattice. Pu^{3+} on Gd and Pu^{4+} on Zr site substitutions in the pyrochlore lattice exhibit a more distinct difference because there is more accommodating free volume at the Gd sites than at the Zr sites (Fig. 3). The fluorite cation–oxygen distances are eightfold at 0.228 nm. The pyrochlore Gd–O distances are twofold at 0.228 nm and sixfold at 0.259 nm, and the Zr–O distances are sixfold at 0.203 nm. The volume and energy changes in Table 6 are therefore consistent with expectations based on ionic radii.

Table 7
Volume and lattice energy changes at 0 K for the fluorite to pyrochlore phase transformation

Case	Volume/atom (%)	Energy/atom (%)
Virgin	9.07	−17.39
10% Pu^{3+}_{Gd}	7.51	−17.67
10% Pu^{4+}_{Zr}	7.99	−17.78

It is reasonable to expect that incorporation of Pu in gadolinium zirconate would be performed at high temperatures where the fluorite phase dominates, the energy requirements are minimized (Table 4), volumetric expansions (Table 6) may be relaxed by higher defect mobilities, and high sintering densities are achieved. Long cooling times may also be anticipated to prevent the accumulation of differential thermal stresses and consequent fractures. Because long cooling times are also associated with the thermal phase transformation from fluorite to pyrochlore [7,24], it is useful to explore the characteristics of this transformation. For this initial investigation, Table 7 shows the volume and energy changes computed by energy minimization at 0 K. Although the smallest energy change is exhibited by the virgin material, it may not be significantly different than for materials containing Pu. The smallest volume changes are exhibited by materials incorporating Pu, with a slight advantage for Pu^{3+} substitutions on Gd sites. This preference is consistent with the above discussion concerning cation–oxygen distances because the more accommodating Gd site shows the lowest volume change.

6. Conclusions

As expected, the simple substitutions of Pu^{3+} on Gd sites and Pu^{4+} on Zr sites exhibit the lowest defect

reaction energies and are, therefore, the ones most likely to occur under reducing or oxidizing conditions, respectively. The exothermic (negative) energies for Pu^{3+} substitutions on Gd sites (and on Zr sites for the fluorite cluster model) may indicate that reducing atmospheres could be beneficial for tightly binding Pu into $Gd_2Zr_2O_7$ hosts. Slightly higher, but still exothermic, defect reaction energies were calculated for Pu^{4+} substitutions on Zr sites for three out of four of the fluorite cases, indicating that oxidizing conditions should not inhibit Pu incorporation into $Gd_2Zr_2O_7$ hosts. Defect reactions involving cation vacancies or interstitials exhibited significantly higher energies, and are therefore not expected to occur. Mean field calculations indicated that volume increases associated with Pu incorporation are minimized by the pyrochlore structure due to the excess of free volume associated with the Gd site in that structure. Volume changes upon thermal phase transformation from fluorite to pyrochlore are smaller for the Pu-containing material than for the virgin material, with a slight advantage for the reducing conditions associated with Pu^{3+} substitutions on Gd sites. The key issues are: (a) the fluorite phase will dominate at high temperatures during waste form processing, (b) the thermal transformation to pyrochlore will be kinetically sluggish during cooling, (c) the transformation-induced volume changes during cooling will be minimized by incorporating Pu, and (d) reducing conditions may offer a slight advantage over oxidizing conditions.

Acknowledgements

This work was supported by the Division of Materials Sciences and Engineering, Office of Basic Energy Sciences, US Department of Energy. The Pacific Northwest National Laboratory is operated by Battelle Memorial Institute for the US Department of Energy under Contract DE-AC06-76RLO 1830. DL_POLY is a package of molecular simulation routines written by W. Smith and T.R. Forester, and copyrighted by the Council for the Central Laboratory of the Research Councils, Daresbury Laboratory at Daresbury, near Warrington (1996). GULP is an atomistic energy minimization code developed by Julian Gale of the Imperial College, London.

Appendix A. Defect reaction equations

Reaction 1. For Pu^{3+} substitution on a Gd^{3+} site:

$$Pu_2O_3 + 2Gd_{Gd} \rightarrow Gd_2O_3 + 2Pu_{Gd}^{3+} \tag{A.1}$$

$$E = 0.5Gd_2O_3^L + Pu_{Gd}^{3+} - 0.5Pu_2O_3^L \tag{A.2}$$

Reaction 2. For Pu^{3+} substitution on a Zr^{4+} site, with charge compensation by oxygen vacancies:

$$Pu_2O_3 + 2Zr_{Zr} + 4O_O \rightarrow 2ZrO_2 + 2Pu_{Zr}^{3+\prime} + V_O^{\cdot\cdot} + 4O_O \tag{A.3}$$

$$E = ZrO_2^L + Pu_{Zr}^{3+\prime} + 0.5V_O^{\cdot\cdot} - 0.5Pu_2O_3^L \tag{A.4}$$

Reaction 3. For Pu^{4+} substitution on a Zr^{4+} site, no charge compensation is needed:

$$PuO_2 + Zr_{Zr} \rightarrow ZrO_2 + Pu_{Zr}^{4+} \tag{A.5}$$

$$E = ZrO_2^L + Pu_{Zr}^{4+} - PuO_2^L \tag{A.6}$$

Reaction 4. For Pu^{4+} substitution on a Gd^{3+} site, with charge compensation by additional oxygens:

$$2PuO_2 + 2Gd_{Gd} \rightarrow Gd_2O_3 + 2Pu_{Gd}^{4+\cdot} + O_{V_O}'' \tag{A.7}$$

$$E = 0.5Gd_2O_3^L + Pu_{Gd}^{4+\cdot} + 0.5O_{V_O}'' - 2PuO_2^L \tag{A.8}$$

Reaction 5. For Pu^{4+} substitution on a Gd^{3+} site, with charge compensation by Gd vacancies:

$$3PuO_2 + 4Gd_{Gd} \rightarrow 2Gd_2O_3 + 3Pu_{Gd}^{4+\cdot} + V_{Gd}'' \tag{A.9}$$

$$E = 0.67Gd_2O_3^L + Pu_{Gd}^{4+\cdot} + 0.33V_{Gd}'' - PuO_2^L \tag{A.10}$$

Reaction 6. For Pu^{3+} substitution on a Zr^{4+} site, with charge compensation by Zr interstitials:

$$2Pu_2O_3 + 4Zr_{Zr} \rightarrow 3ZrO_2 + 4Pu_{Zr}^{3+\prime} + Zr_i^{''''} \tag{A.11}$$

$$E = 0.75ZrO_2^L + Pu_{Zr}^{3+\prime} + 0.25Zr_i^{''''} - 0.5Pu_2O_3^L \tag{A.12}$$

Reaction 7. For mixed Pu^{3+} substitution on a Gd^{3+} site and Pu^{3+} interstitials, with charge compensation by Gd vacancies:

$$Pu_2O_3 + 2Gd_{Gd} \rightarrow Gd_2O_3 + Pu_{Gd}^{3+} + Pu_i^{3+\cdots} + V_{Gd}''' \tag{A.13}$$

$$E = Gd_2O_3^L + Pu_{Gd}^{3+} + Pu_i^{3+\cdots} + V_{Gd}''' - Pu_2O_3^L \tag{A.14}$$

Reaction 8. For Pu^{3+} interstitials, with charge compensation by additional oxygens:

$$Pu_2O_3 \rightarrow 2Pu_i^{3+\cdots} + 3O_{V_O}'' \tag{A.15}$$

$$E = Pu_i^{3+\cdots} + 1.5O_{V_O}'' - 0.5Pu_2O_3^L \tag{A.16}$$

Reaction 9. For Pu^{4+} interstitials and substitutions on a Zr^{4+} site, with charge compensation by zirconium vacancies:

$$2PuO_2 + 2Zr_{Zr} \rightarrow 2ZrO_2 + Pu_i^{4+\cdots\cdot} + V_{Zr}^{''''} + Pu_{Zr}^{4+} \quad (A.17)$$

$$E = ZrO_2^L + 0.5Pu_i^{4+\cdots\cdot} + 0.5V_{Zr}^{''''} + 0.5Pu_{Zr}^{4+} - PuO_2^L \quad (A.18)$$

Reaction 10. For Pu^{4+} interstitials with charge compensation by additional oxygens:

$$PuO_2 \rightarrow Pu_i^{4+\cdots\cdot} + 2O_{V_O}'' \quad (A.19)$$

$$E = Pu_i^{4+\cdots\cdot} + 2O_{V_O}'' - PuO_2^L \quad (A.20)$$

Reaction 11. For Pu^{3+} interstitials, with charge compensation by Gd vacancies:

$$Pu_2O_3 + 2Gd_{Gd} \rightarrow Gd_2O_3 + 2Pu_i^{3+\cdots} + 2V_{Gd}'' \quad (A.21)$$

$$E = 0.5Gd_2O_3^L + Pu_i^{3+\cdots} + V_{Gd}'' - 0.5Pu_2O_3^L \quad (A.22)$$

Reaction 12. For Pu^{4+} interstitials, with charge compensation by zirconium vacancies (Frenkellike):

$$PuO_2 + Zr_{Zr} \rightarrow ZrO_2 + Pu_i^{4+\cdots\cdot} + V_{Zr}'''' \quad (A.23)$$

$$E = ZrO_2^L + Pu_i^{4+\cdots\cdot} + V_{Zr}'''' - PuO_2^L \quad (A.24)$$

References

[1] K.K.S. Pillay, Radwaste (1996) 60.
[2] G. Taubes, Science 263 (1994) 629.
[3] V.M. Oversby, C.C. McPheeters, C. Degueldre, J.M. Paratte, J. Nucl. Mater. 245 (1997) 17.
[4] D.M. Strachan, R.D. Scheele, W.C. Buchmiller, J.D. Vienna, R.L. Sell, R.J. Elovich, Preparation and Characterization of 238Pu–Ceramics for Radiation Damage Experiments, PNNL-13251 (2000) Pacific Northwest National Laboratory, Richland, WA, USA.
[5] W.J. Weber, J.W. Wald, Hj. Matzke, Mater. Lett. 3 (1985) 173.
[6] W.J. Weber, J.W. Wald, Hj. Matzke, J. Nucl. Mater. 138 (1986) 196.
[7] S.X. Wang, B.D. Begg, L.M. Wang, R.C. Ewing, W.J. Weber, K.V. Govidan Kutty, J. Mater. Res. 14 (1999) 4470.
[8] K.E. Sickafus, L. Minervini, R.W. Grimes, J.A. Valdez, M. Ishamaru, F. Li, J. McClellan, T. Hartmann, Science 289 (2000) 748.
[9] R.E. Williford, B.D. Begg, W.J. Weber, N.J. Hess, J. Nucl. Mater. 278 (1999) 207.
[10] J.D. Gale, J. Chem. Soc., Faraday Trans. 93 (1997) 629.
[11] J.D. Gale, Philos. Mag. B 73 (1996) 3.
[12] N.F. Mott, M.J. Littleton, Trans. Faraday Soc. 34 (1938) 485.
[13] B.G. Dick, A.W. Overhauser, Phys. Rev. 112 (1958) 90.
[14] W. Hayes, A.M. Stoneham, Defects and Defect Processes in Nonmetallic Solids, Wiley, New York, 1985.
[15] T.R. Forester, W. Smith, The DL_POLY code, Daresbury Laboratory, UK, 1993.
[16] A. Dwivedi, A.N. Cormack, J. Solid State Chem. 79 (1989) 218.
[17] R.E. Williford, R. Devanathan, W.J. Weber, J.D. Gale, in: V.V. Bulatov, T. Diaz de la Rubia, R. Phillips, E. Kaxrias, N. Ghoneim (Eds.), Multiscale Modeling of Materials, Mater. Res. Soc. Symp. Proc., vol. 538, Material Research Society, Warrendale, PA, 1999, p. 235.
[18] R.E. Williford, W.J. Weber, R. Devanathan, J.D. Gale, J. Electroceram. 3 (4) (1999) 409.
[19] R.E. Williford, W.J. Weber, J. Am. Ceram. Soc. 82 (1999) 3266.
[20] http//www.caos.kun.nl.
[21] P.E. Raison, R.G. Haire, T. Sato, T. Ogawa, in: Mater. Res. Soc. Symp. Proc., vol. 556, Material Research Society, Warrendale, PA, 1999, p. 3.
[22] R.S. Roth, T. Negas, L.P. Cook, in: Phase Diagrams for Ceramists, vol. 4, American Ceramic Society, Columbus, OH, 1981, p. 129.
[23] K.B. Helean, B.D. Begg, A. Navrotsky, B. Ebbinghaus, W.J. Weber, R.C. Ewing (in press).
[24] P.K. Moon, H.L. Tuller, in: G. Nasri, R.A. Huggins, D.F. Shriver (Eds.), Solid State Ionics, Mater. Res. Symp. Proc., Pittsburgh, PA, vol. 135, 1989, p. 149.
[25] R.D. Shannon, Acta. Crystallogr. A 32 (1976) 751.